AFRL-RW-EG-TP-2009-7030

Evaluation of the haltere as a biologically-inspired inertial rate sensor

R. A. Thompson, M. F. Wehling, J. E. Evers
Air Force Research Laboratory
Munitions Directorate
AFRL/RWGI
Eglin AFB, FL 32542-6810

W. E. Dixon
Dept. of Mechanical and Aerospace Engineering
University of Florida
Gainesville, FL 32611

MARCH 2009

CONFERENCE PAPER

AIR FORCE RESEARCH LABORATORY, MUNITIONS DIRECTORATE

■ **Air Force Materiel Command** ■ **United States Air Force** ■ **Eglin Air Force Base**

REPORT DOCUMENTATION PAGE

Form Approved
OMB No. 0704-0188

PLEASE DO NOT RETURN YOUR FORM TO THE ABOVE ADDRESS.

1. REPORT DATE *(DD-MM-YYYY)*	2. REPORT TYPE	3. DATES COVERED *(From - To)*
24 March 2009	Technical Paper	January 2008 to March 2009

4. TITLE AND SUBTITLE

Evaluation of the haltere as a biologically-inspired inertial rate measurement sensor

5a. CONTRACT NUMBER

NA

5b. GRANT NUMBER

NA

5c. PROGRAM ELEMENT NUMBER

PE602602F

6. AUTHOR(S)

R. A. Thompson
M. F. Wehling
J. E. Evers
W. E. Dixon

5d. PROJECT NUMBER

2068

5e. TASK NUMBER

82

5f. WORK UNIT NUMBER

01

7. PERFORMING ORGANIZATION NAME(S) AND ADDRESS(ES)

Air Force Research Laboratory
Munitions Directorate
AFRL/RWGI
Eglin AFB, FL 32542-6810

8. PERFORMING ORGANIZATION REPORT NUMBER

AFRL-RW-EG-TP-2009-7030

9. SPONSORING/MONITORING AGENCY NAME(S) AND ADDRESS(ES)

Air Force Research Laboratory
Munitions Directorate
AFRL/RWGI
Eglin AFB, FL 32542-6810

10. SPONSOR/MONITOR'S ACRONYM(S)

AFRL-RW-EG

11. SPONSOR/MONITOR'S REPORT NUMBER(S)

SAME AS BLOCK 8

12. DISTRIBUTION/AVAILABILITY STATEMENT

DISTRIBUTION A: Approved for public release; distribution unlimited.
Approval Confirmation 96 ABW/PA # 02-25-08-087; dated 25 February 2008.

13. SUPPLEMENTARY NOTES

See 'cover page' for pertinent metadata information.

14. ABSTRACT

Since as early as the 1940's, specialized structures on dipteran insects have been recognized as necessary for inertial measurement associated with basic flight stability. These structures, called halteres, have been suggested to act as vibrating structure gyroscopes, measuring strains proportional to Coriolis accelerations. As a miniature, robust means for stabilizing flight, this biological inertial measurement system is not only of interest to biologists, but also to designers of biomimetic robotic systems. However, the accuracy with which a pair of halteres can reconstruct the full body rate vector had not been clearly ascertained in previous studies. In addition, only one potential mechanism to decouple the rate components, using frequency decomposition of the haltere mechanical response, has been generally adopted. The purpose of this paper is to present an evaluation of the halteres as a rate measurement sensor through dynamic simulation of the halteres across a full range of body angular rates. Based on this analysis, a simple alternative mechanism is proposed for decoupling the body rate components, and, assuming the use of this proposed mechanism, an error analysis is presented for the halteres as a three dimensional linear rate measurement system.

15. SUBJECT TERMS

diptera - haltere - flight stability - strain rate - campaniform sensilla

16. SECURITY CLASSIFICATION OF:			17. LIMITATION OF ABSTRACT	18. NUMBER OF PAGES	19a. NAME OF RESPONSIBLE PERSON
a. REPORT	b. ABSTRACT	c. THIS PAGE			M. F. Wehling
UNCLASSIFIED	UNCLASSIFIED	UNCLASSIFIED	SAR	14	19b. TELEPHONE NUMBER *(Include area code)*

Evaluation of the haltere as a biologically inspired inertial rate measurement sensor

R. A. Thompson, M. F. Wehling, J. Evers
Air Force Research Laboratory (AFRL/RWG), Eglin AFB, FL 32542

W. E. Dixon
Dept. of Mechanical and Aerospace Engineering, Univ. of Florida, Gainesville, FL 32611

Since as early as the 1940's, specialized structures on dipteran insects have been recognized as necessary for inertial measurement associated with basic flight stability. These structures, called halteres, have been suggested to act as vibrating structure gyroscopes, measuring strains proportional to Coriolis accelerations. As a miniature, robust means for stabilizing flight, this biological inertial measurement system is not only of interest to biologists, but also to designers of biomimetic robotic systems. However, the accuracy with which a pair of halteres can reconstruct the full body rate vector had not been clearly ascertained in previous studies. In addition, only one potential mechanism to decouple the rate components, using frequency decomposition of the haltere mechanical response, has been generally adopted. The purpose of this paper is to present an evaluation of the halteres as a rate measurement sensor through dynamic simulation of the halteres across a full range of body angular rates. Based on this analysis, a simple alternative mechanism is proposed for decoupling the body rate components, and, assuming the use of this proposed mechanism, an error analysis is presented for the halteres as a three dimensional linear rate measurement system.

Introduction

Collaboration between engineers and biologists continues to increase due to the continual pressure on engineers to build smaller, more robust, and intelligent systems. Such systems are plentiful in the realm of biology, with seemingly unlimited variations resulting from genetic propagation of specific forms that offer some advantage in a continuously changing environment. Engineers have developed a particular interest in insects due to the great diversity of sensors that could be emulated to allow enabling capabilities for missions such as autonomous surveillance and tracking. The optical sensors on some insects can change sensitivity by three orders of magnitude within minutes of changing light conditions. Insects are also known to distinguish up to four regions of the electromagnetic spectrum and to take advantage of polarization characteristics of light for navigation[1].[2] Insects have sensors that measure gravitational direction,[3] inertial state, and chemical signatures. To enable locomotion and propulsion, mechanoreceptive and proprioceptive sensors are embedded throughout the exoskeleton to measure position, locations, and rates of motion of the various appendages, as well as the motion of the overall body with respect to the environment. These sensors, along with the associated power generation and control functions, tantalize the engineer by being packaged in body sizes as small as a fraction of a millimeter in the case of some parasitic wasp and fly species.

A contribution of this paper is an analysis of the dynamics of the haltere, a sensor which was first observed to play a role in flight stabilization by Derham in the early 18th century. It was not until the late 1930's that researchers such as Pringle[4] began to characterize the dynamic forces acting on the haltere and thereby firmly establishing the role of the haltere as a gyroscopic mechanism, sensing Coriolis forces proportional to body rates. Pringle demonstrated the feasibility of the haltere (see Fig. 1) as an angular rate sensor used to stabilize the body of dipteran (two winged) insects during flight. Proof of this function is apparent when the halteres, which are small genetically inhibited[5] adaptations of the rear wings, are removed, rendering the fly unable to maintain stable flight.[4] The halteres are much too small to generate significant aerodynamic forces, and therefore it was deduced that they have adapted to provide body motion state feedback to the

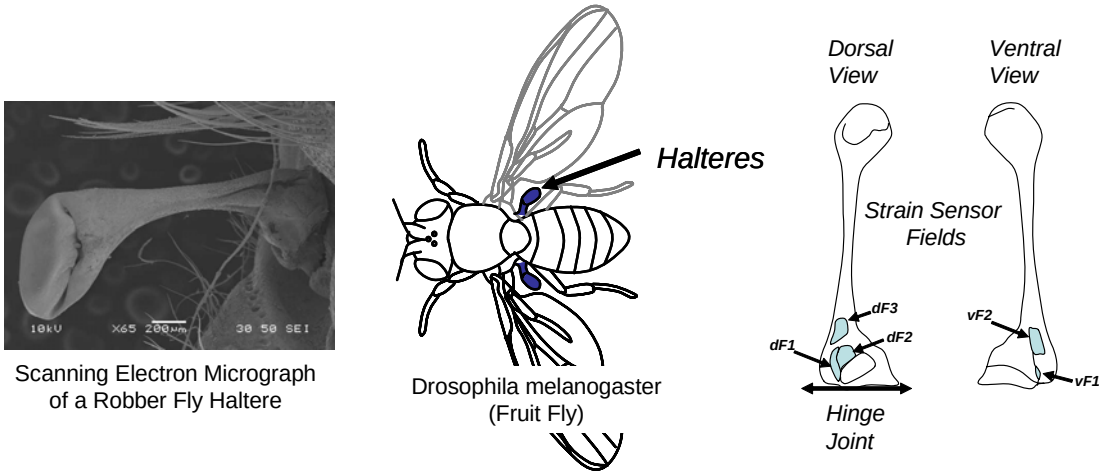

Figure 1. Characteristic locations of the halteres and their strain sensors.

fly's control system. Due to their common lineage, the fully developed wings have a similar configuration of muscles and the same type of strain sensors as the halteres, and therefore may also measure and feedback signals that are in part representative of the state of inertial motion. However, the wings have relatively large aerodynamic and inertial forces that might contaminate measurement of the induced Coriolis force, so they would likely be much less predominant for that function if halteres are present.

Halteres and the associated control functions have been studied by a number of authors. Some of the most recent work by Dickinson[67] has focused on the interaction between the halteres and both the flight control functions of the wings and the visual sensors on the head. The haltere has also been investigated by some researchers as a biomimetic inertial measurement instrument. For example, Wu and Wood[8] have patented a mechanical haltere, claiming that halteres offer advantages that other methods of inertial sensing do not. Some conject that the original works by Fraenkel and Pringle[94] were the inspiration for the modern micro-electro-mechanical (MEMS) vibrating mass gyroscopes that are now available with a unit cost of less than $100. These MEMS gyros can be seen in a variety of applications, including commercial automobile braking systems, modern avionics, and skegways. The halteres, unlike the technologies they may have inspired, are large amplitude systems, oscillating back and forth through a range of up to +/- 90 degrees. Therefore, a single haltere offers the potential to measure rates of change of angular orientation in at least two orthogonal directions, similar to a vibrating disk gyroscope or a conventional spinning mass gyroscope.

The physical mechanism that allows halteres to measure angular rate is associated with the motion of the mass at the end of the haltere as it oscillates in a plane that is roughly fixed relative to the body of the insect. If the insect, and therefore the attached plane, is allowed to rotate in inertial space, then the moving mass is generally required to accelerate to stay in the plane. This acceleration is due to the change in direction of the velocity vector caused by the rotation of the plane and the change in the radial location of the mass relative to the axis of rotation. The combination of these effects (i.e., $2({}^e\overrightarrow{\omega}^b \times {}^b\overrightarrow{v}^m)$) is referred to as the Coriolis acceleration, and the magnitude is proportional to the component of velocity in the rotating reference frame that is perpendicular to the bodies angular velocity vector.

If two angular velocity vector components are in the plane of the haltere, see Figure 2, the velocity of the haltere mass perpendicular to the transverse component Ω_y will change sign once during a complete cycle of the haltere motion. However, the component of the velocity perpendicular to the medial component Ω_x will change sign twice. The end result is that the signal (force, displacement, strain, etc.) coming from the haltere due to the medial component will have twice the frequency of the signal resulting from the transverse component of the angular velocity. The implication of the early analysis was that insects using halteres could possibly do a frequency decomposition of the mechanoreceptive nerve signals in order to resolve the two rate components. This is the basis for the patent of Wu and Wood.[8] The remainder of this paper will show that it is also possible, if the mechanoreceptive sensors could measure the appropriate quantities, to measure the same two components by taking advantage of the natural decoupling of the rate components at the center

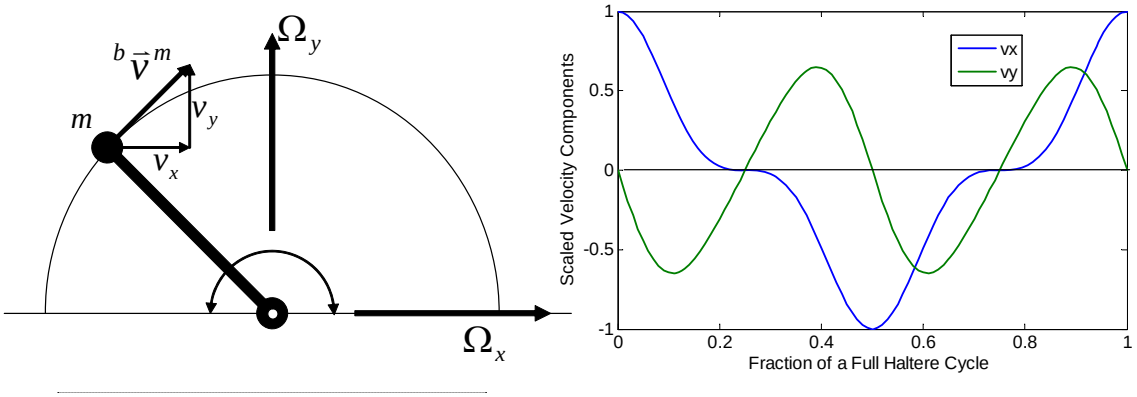

Figure 2. As the haltere beats back and forth the velocity component perpendicular to Ω_x changes sign at twice the frequency as the component perpendicular to Ω_y. This results in a Coriolis force with two distinct frequency components.

of the haltere stroke and the approximately linear nature of the governing equation of motion. In addition, results of an error analysis will be given from which the relative errors inherent in the measurement of all three body rate components can be inferred due to the nonlinearities in the "true" equations of motion.

I. Model Description

Dickinson's work on haltere mediated reflexes describes the physical geometry of the fruit fly, *Drosophila melanogaster*.[10] This description of the geometry, see Fig. 3, is used as a starting point for the haltere analysis in this paper. The predominant characteristics of the biological system used in the current development are the amplitude of the haltere stroke and the configuration of the halteres with respect to the mid-sagittal and transverse planes of the fly body. The halteres on *Drosophila* oscillate in a plane that is tilted back roughly thirty degrees toward the mid-sagittal plane. The line that defines the intersection of the haltere stroke plane with the sagittal plane is rotated toward the head by roughly twenty degrees so that at the top of its stroke the tip of the haltere is in a more anterior position than at the bottom of the stroke as shown in Fig. 3. However, since the line of intersection of the haltere planes is, for convenience, used to define the body yaw axis ($\hat{x}_3$), the value of this angle is arbitrary. The beat frequency was rounded up to 200 Hz from the described range of 150 to 180 Hz for the sake of analytical convenience in simulations where general trends of out-of-plane stiffness and damping impact on the trajectory were simulated.

The equations of motion are non-dimensional and describe the system in terms of its natural frequency and damping coefficient, as opposed to using dimensional quantities to describe mass, length, damping and stiffness characteristics. The component of the haltere motion in the primary plane of oscillation is assumed to be deterministic and purely harmonic as observed in the body reference frame, oscillating back and forth through a range of +/-ninety degrees. Damping of out-of-plane motion is assumed to be proportional to the angular rate of the out-of-plane motion and the stiffness proportional to out-of-plane displacement. The source of stiffness is not specified, whether it is due to the resiliency of the haltere stalk or the joint and its associated musculature. The haltere model for out-of-plane motion can be considered as an equivalent mass at the radius of gyration of the haltere on a rigid massless structure with a torsional spring and damper at the base. The actual dynamics and control of the haltere may be much more complex and is an area of ongoing research. Hengstenberg[11] describes eleven control muscles at the base of the haltere similar to the muscles at the base of the wing. These muscles could possibly fine tune the kinematics of the haltere.

The equations of motion are generated without any small angle assumptions for the purpose of simulating the haltere trajectory under the influence of constant inertial body rates. Transients are not considered in this phase of the research and only the haltere response under the ideal conditions of constant angular rate were examined to draw preliminary conclusions about the fundamental limitations of the haltere or haltere pair. This steady-state assumption is equivalent to assuming that the body rates have a significantly longer period than the period of haltere oscillation and any associated transients.

Finally, the component of angular rotation of the haltere in its primary plane is assumed to be sinusoidal.

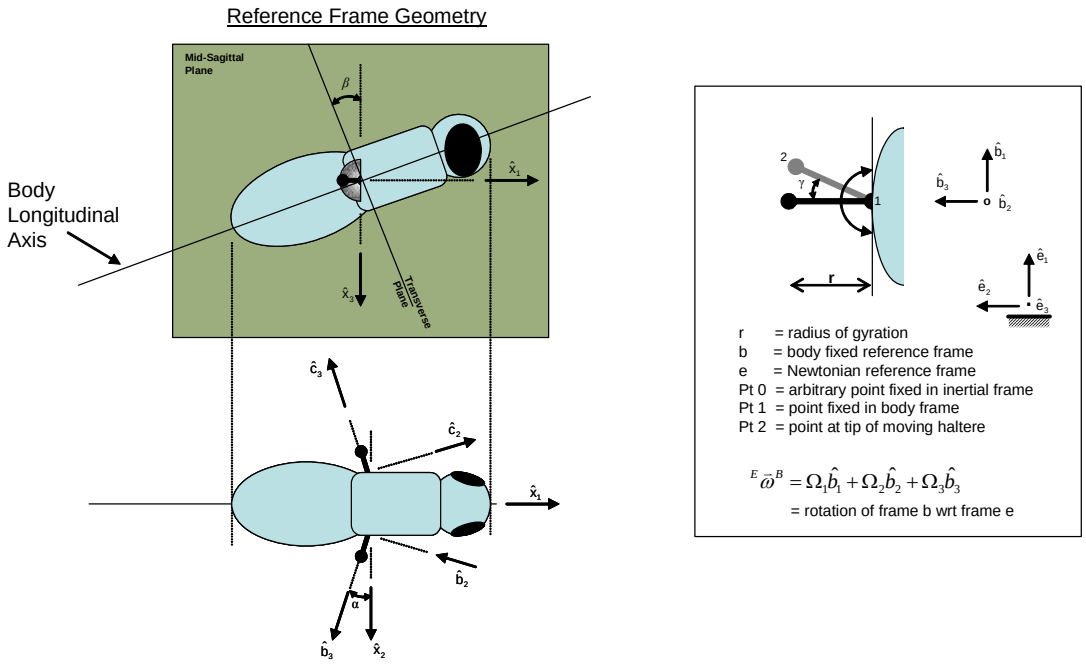

Figure 3. Reference frame definitions for the halteres, b and c, and frame x which defines the roll (x_1), pitch (x_2) and yaw (x_3) axis. The angle beta is arbitrary with this definition of reference frames.

That is, the angular position γ of the haltere in its primary plane of motion is assumed to be

$$\gamma = \frac{\pi}{2}\sin(\omega t),$$

where ω is the constant beat frequency of the haltere. The sinusoidal assumption is not valid for insects that have a flatter angular velocity profile for the majority of the stroke and a quicker turn around at the ends. Yet, this assumption can be used to develop valid conclusions as long as the haltere maintains its symmetry of motion with respect to the center of the stroke.

II. Kinematic Assessment

Insight regarding the forces acting in the out-of-plane direction can be examined by first assuming no out-of-plane haltere deflection. The right half of Fig. 3 shows the right haltere and reference frame directions associated with the haltere and inertial space. In the following sections, hatted variables represent unit vectors that describe orthogonal directions for the required reference frames. Left superscripts describe which reference frame the vector quantity is observed within. Right superscripts identify the point or reference frame the quantity characterizes. The body angular rate vector relative to the inertial frame, ${}^e\vec{\omega}^b = {}^e\vec{\omega}^x$, is represented in the right haltere reference frame as

$${}^e\vec{\omega}^b = \Omega_1\hat{b}_1 + \Omega_2\hat{b}_2 + \Omega_3\hat{b}_3. \tag{1}$$

In this expression, Ω_i are the angular velocity components and $\hat{b}_i$ are the body fixed unit vectors as shown in Fig. 3**.** The position, velocity and acceleration of a point mass at the radius of gyration of the haltere are found through successive differentiation to be:

$$\vec{P}_{02} = \vec{P}_{01} + \vec{P}_{12} \tag{2}$$

$${}^e\vec{v}^2 = {}^e\vec{v}^1 + {}^b\vec{v}^2 + {}^e\vec{\omega}^b \times \vec{P}_{12} \tag{3}$$

$${}^e\vec{a}^2 = {}^e\vec{a}^1 + {}^b\vec{a}^2 + 2({}^e\overrightarrow{\omega}^b \times {}^b\vec{v}^2) + {}^e\overrightarrow{\omega}^b \times ({}^e\overrightarrow{\omega}^b \times \vec{P}_{12}) + {}^e\overrightarrow{\alpha}^b \times \vec{P}_{12}. \tag{4}$$

In these expressions, 0,1 and 2 refer to an arbitrary point fixed in inertial space, a point at the base of the haltere, and a point at the radius of gyration of the haltere, respectively. The first acceleration term, ${}^e\vec{a}^1$, which is the acceleration of the base of the haltere with respect to the inertial frame is assumed to be small. The second term, ${}^b\vec{a}^2$, which represents acceleration of the haltere mass as observed from the body, is entirely in the plane of the haltere. Nalbach[12] showed that these primary accelerations in the plane-of-motion are much higher than contributions associated with the body angular rates, and therefore, useful information pertaining to the body rates is unlikely to be ascertained from in-plane force measurements. The last term, ${}^e\overrightarrow{\alpha}^b \times \vec{P}_{12}$, which involves the angular acceleration of the body, was also shown by Nalbach to be a factor of 5 or more less than the third (Coriolis) term for sinusoidal body oscillations under fifty Hz. The remaining two terms after taking the appropriate vector products are

$$2({}^e\overrightarrow{\omega}^b \times {}^b\overrightarrow{v}^2) = 2r\dot{\gamma}[-\Omega_2\sin(\gamma)\hat{b}_1 + (\Omega_1\sin(\gamma) + \Omega_3\cos(\gamma))\hat{b}_2 - \Omega_2\cos(\gamma)\hat{b}_3] \quad (5)$$

$$\begin{aligned} {}^e\overrightarrow{\omega}^b \times ({}^e\overrightarrow{\omega}^b \times \vec{P}_{12}) = {} & r[(-\Omega_2^2\sin(\gamma) - \Omega_3^2\sin(\gamma) + \Omega_1\Omega_2\cos(\gamma))\hat{b}_1 + \\ & (\Omega_1\Omega_2\sin(\gamma) + \Omega_2\Omega_3\cos(\gamma))\hat{b}_2 + \\ & (\Omega_1\Omega_3\sin(\gamma) - \Omega_1^2\cos(\gamma) - \Omega_2^2\cos(\gamma))\hat{b}_2]. \end{aligned} \quad (6)$$

The expression in (5) is the Coriolis term which generates out-of-plane ($\hat{b}_2$) force components associated with the in-plane body rates. These components are proportional to $2\dot{\gamma}\Omega_1$ and $2\dot{\gamma}\Omega_3$. The other components represent an in-plane acceleration directed along the stalk of the haltere proportional to Ω_2. The expression in (6) describing the centripetal accelerations, also generates out-of-plane forces on the haltere proportional to $\Omega_1\Omega_2$ and $\Omega_2\Omega_3$.The relative magnitudes of $\dot{\gamma}$ and Ω_2 will determine the significance of these centripetal terms. Errors introduced by these terms will be quantified later in the paper. If the centripetal terms are small, we would expect the out-of-plane force on the haltere should predominantly be due to the Coriolis term and therefore is associated with the body rate components that are in the primary plane of the haltere motion. Equations (5) and (6) are based on the assumption that the haltere is infinitely rigid and does not deflect out-of-plane. This assumption is the basis for the previous kinematic analysis of the haltere by Pringle and Nalbach and is useful for developing an intuition regarding the predominant forces that impact the problem. In the following section, this assumption is eliminated to simulate the out-of-plane motion, or equivalently the strains resulting from that motion.

If the halteres are assumed to measure forces associated with the Coriolis accelerations, the measured signals should be proportional to the in-plane body rate components, $\Omega_1$and Ω_3, as shown in (5). If two halteres that are initially in a common plane are rotated out of the plane by an angle α as shown in Fig. 3, then all three components of the body inertial rate vector can be reconstructed. The body rate vector represented in the body fixed roll, pitch, yaw frame is

$${}^e\vec{\omega}^x = W_1\hat{x}_1 + W_2\hat{x}_2 + W_3\hat{x}_3, \quad (7)$$

where W_1, W_2 and W_3 are the body roll, pitch, and yaw rates, respectively[a].

The relationships between the components of the body rate vector represented in the body roll, pitch, yaw frame and the components represented in the right haltere frame ($\hat{b}$) and the left haltere frame ($\hat{c}$) are

$$\begin{aligned} {}^e\vec{\omega}^x &= \Omega_{b1}\hat{b}_1 + \Omega_{b2}\hat{b}_2 + \Omega_{b3}\hat{b}_3 \\ &= \Omega_{c1}\hat{c}_1 + \Omega_{c2}\hat{c}_2 + \Omega_{c3}\hat{c}_3 \end{aligned} \quad (8)$$

$$W_1 = -\frac{\Omega_{b3} + \Omega_{c3}}{2\sin(\alpha)} \quad (9)$$

$$W_2 = \frac{\Omega_{b3} - \Omega_{c3}}{2\cos(\alpha)} \quad (10)$$

$$W_3 = -\frac{\Omega_{b1} + \Omega_{c1}}{2} = -\Omega_{b1} = -\Omega_{c1} \quad (11)$$

The importance of these simple transformations is that they allow a direct calculation of rate components along the body roll, pitch, and yaw axes, W_1, W_2 and W_3, given the two rate components that are measurable

[a] The terms roll, pitch and yaw are used in this paper to indicate the body rate components, commonly referred to as p,q and r, as opposed to sequence dependent Euler angle rates. These are equivalent if the body and inertial frame are co-aligned at the instant at which the rates are described.

in each of the haltere reference frames. The research on halteres by Pringle[4] in 1948 did not recognize the ability of the insect physiology to combine the output of two halteres and thereby distinguish between pitch and roll components of the body rate vector. Pringle initially assumed that the halteres represented a redundant means of measuring yaw rate. Later experimental results by Faust[13] demonstrated the ability of flies to react independently to each of the body rates. Therefore, within the neurology of dipteran insects there is likely a basic representation of (9)-(11), although this does not rule out measurements from other sensors that support inertial stabilization.

III. Dynamics Equation Allowing for Out-of-Plane Motion

For the purpose of simulating the dynamics of the haltere, out-of-plane motion is considered. With the out-of-plane deflection angle defined as θ, summing moments associated with damping, stiffness, and inertial forces around the base of the haltere results in the following expression:

$$\begin{aligned}\ddot{\theta} + 2\zeta\omega_n\dot{\theta} + \omega_n^2\theta &= \dot{\Omega}_3\sin(\gamma) - \dot{\Omega}_1\cos(\gamma) - \dot{\gamma}^2\cos(\theta)\sin(\theta) \\ &+2\dot{\gamma}[(\Omega_3\cos(\gamma) + \Omega_1\sin(\gamma))\cos^2(\theta) - \Omega_2\cos(\theta)\sin(\theta)] \\ &+(\Omega_3^2\cos^2(\gamma) + \Omega_1^2\sin^2(\gamma) - \Omega_2^2)\cos(\theta)\sin(\theta) \\ &+(\Omega_2\Omega_3\cos(\gamma) + \Omega_1\Omega_2\sin(\gamma))\cos(2\theta) \\ &+2\Omega_1\Omega_3\cos(\theta)\sin(\theta)\cos(\gamma)\sin(\gamma).\end{aligned} \tag{12}$$

In (12), ζ is the damping ratio, and ω_n is the natural frequency that characterizes the out-of-plane stiffness and mass characteristics of the haltere. In this form, the haltere can be easily simulated by varying the out-of-plane natural frequency relative to the haltere beat frequency as well as varying the haltere damping characteristics. Again, the haltere stroke angle is assumed to vary with a simple characteristic motion $\gamma = \frac{\pi}{2}\sin(w_h t)$, with the angular frequency of the haltere, $w_h = 200Hz$. The derivation of (12) is described in the appendix. This relationship is closely related to the governing equation for the vibrating structure MEMS gyroscope.[b]

IV. Haltere Trajectories

Simulations of the developed equation of motion were executed for a variety of cases with variations in the damping ratio and out-of-plane stiffness. The intent was to determine the characteristics of the displacement trajectories and the impact of non-linear coupling of out-of-plane rate components into the in-plane component measurements. All simulations were executed with constant body rates. For the purpose of generating the plots, the haltere motion was initiated with no out-of-plane displacement and the haltere was allowed to transiently respond to the forces resulting from input body rates. The simulation was executed for 40 oscillations, with the last 20 used for making the plots. Because the haltere has reached a steady state trajectory, the 20 oscillations overlap, appearing as one closed loop. Only for cases where the out-of-plane natural frequency was significantly less than the haltere oscillation frequency, or for cases where the damping was very low did the haltere not reach steady state. These plots are not shown since they represent very large out-of-plane motion for the assumed model, which would not be representative of the evolved system.

IV.A. Out-of-Plane Stiffness Variations

Figures 4 and 5 show the trajectories associated with a haltere out-of-plane natural frequency equal to and double the beat frequency of 200 Hz. The plot shows out-of-plane displacement in radians as the ordinate, plotted against the stroke angle of the haltere as the abscissa. A haltere stroke angle of 0 has the haltere at the center of the stroke. The Ω_1 input generates the expected frequency doubled signal as the haltere sweeps through a semi-circular arc causing the velocity component perpendicular to Ω_1 to change sign twice, therefore the Coriolis force changes sign twice. In the other direction the haltere velocity perpendicular to Ω_3 only changes sign once, giving no frequency doubling effect. The angular displacements peak at

[b] For the case where both θ and γ are much less than 1, damping is small, $\omega_n^2 \gg Amp^2\omega_h^2$, and $\omega_n^2 \gg \omega_h^2$, equation 12 reduces to $\ddot{\theta} + \omega_n^2\theta = 2\Omega_3\dot{\gamma} = 2\Omega_3 A\omega_h\cos(\omega_h t)$. The forced solution to this equation, ($\theta = \frac{2\Omega_3 A\omega_h}{\omega_n^2}\cos(\omega_h t)$), is the solution for the out-of-plane displacement of the MEMS gyro mechanism.

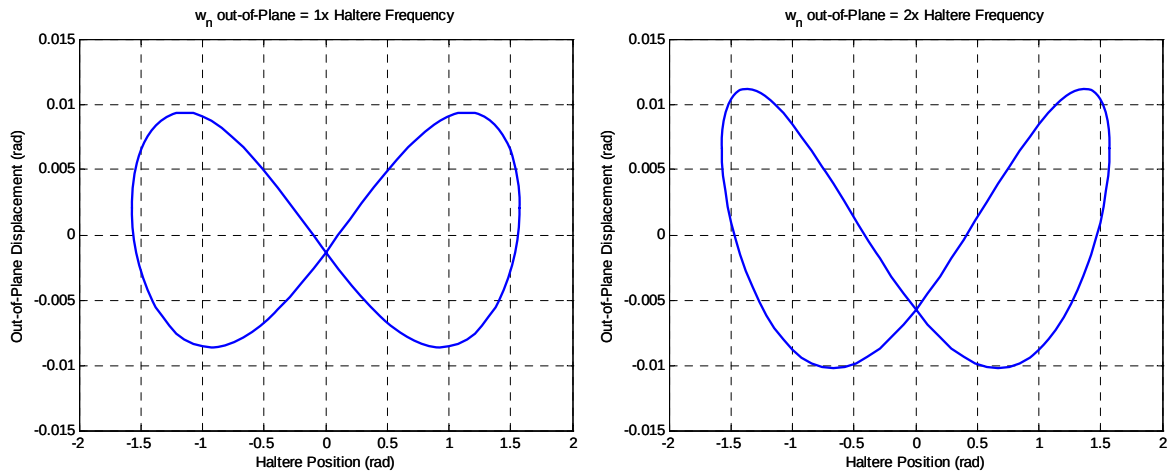

Figure 4. Haltere trajectories for $\omega_n = 200Hz$ (left) and $\omega_n = 400Hz$ (right). Input conditions $\Omega_1 = 10\ \ rad/s$, $\Omega_2 = \Omega_3 = 0$ and $\zeta = 0.1$.

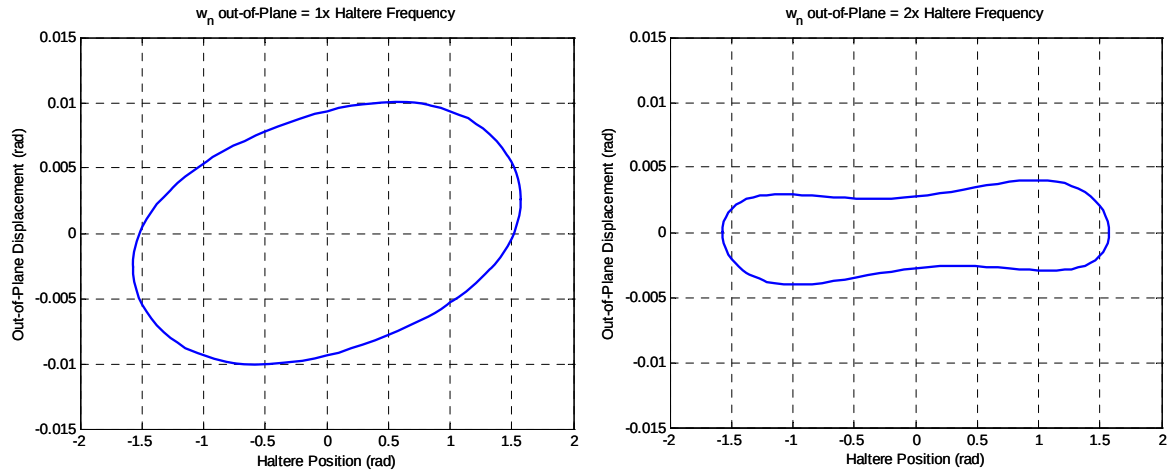

Figure 5. Haltere trajectories for $\omega_n = 200Hz$ (left) and $\omega_n = 400Hz$ (right). Input conditions $\Omega_3 = 10\ \ rad/s$, $\Omega_1 = \Omega_2 = 0$ and $\zeta = 0.1$.

approximately half of a degree for the conditions shown. When the natural frequency is significantly below 200 Hz, the out-of-plane motion is driven to very large angles and never reaches a steady state pattern.

IV.B. Damping Variations

Examples of damping variations are shown in Figure 6 for the case of $\omega_n = 200Hz$ and input body rates of $\Omega_1 = \Omega_3 = 10\ \ rad/s$. These plots demonstrate the significant impact that damping variations, whether passively or actively induced, can have on the haltere trajectory. At low damping levels, $\zeta \approx 0.01$, the trajectory never reached steady state within the forty oscillation (0.2 second) simulation time.

IV.C. Average Haltere Position

The haltere displacement averaged with respect to haltere stroke angle is also shown in Figure 6. However, when the average displacement is plotted seperately for the two rate components as in Figure 7, an interesting characteristic emerges that may provide insight into a possible mechanism by which the body rates are decoupled by the insect.

Figure 7 demonstrates a natural decoupling of the body rate components at the center of the haltere

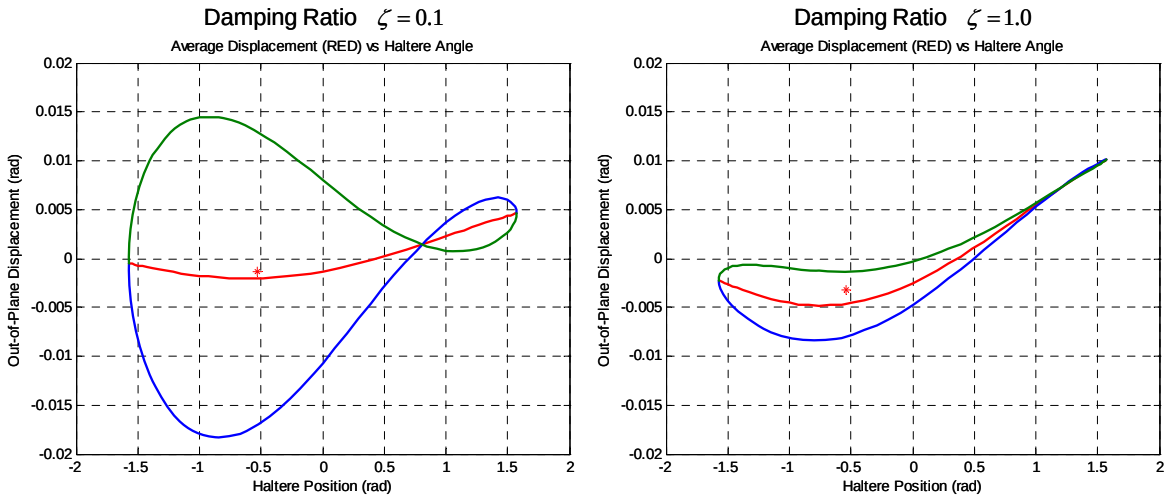

Figure 6. Haltere trajectories with damping ratios at 10% of critical (left) and 100% critical (right) for body rate inputs of $\Omega_1 = \Omega_3 = 10 \ \ rad/s$.

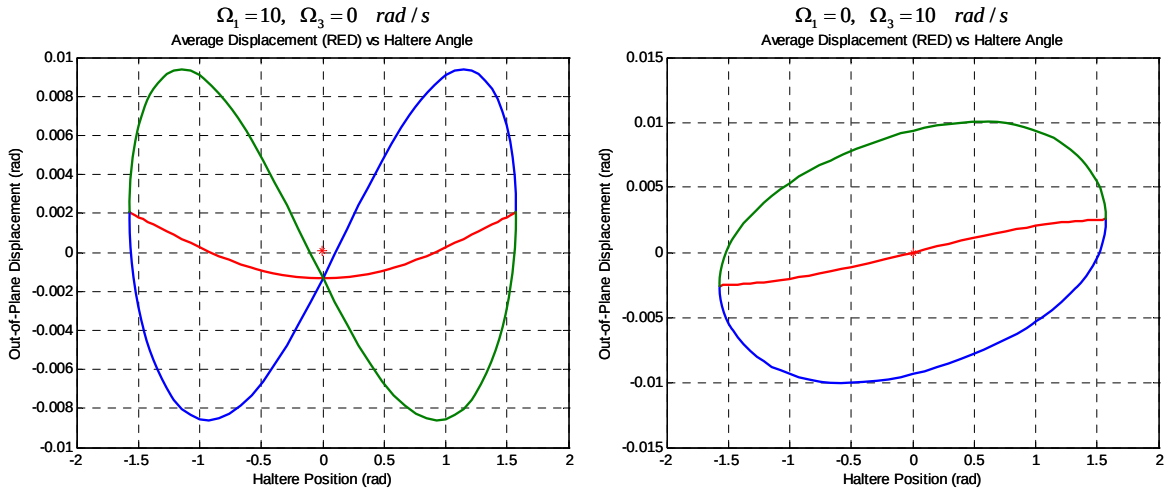

Figure 7. Haltere trajectories for $\Omega_1 = 10 \ \ rad/s$ (top) and $\Omega_3 = 10 \ \ rad/s$ (bottom) with the average displacement plotted as a function of stroke angle.

stroke. At $\gamma = 0$, the averaged magnitude of the response driven by Ω_3 is zero and the averaged slope of the response driven by $\Omega_1$is zero. If the governing differential equation (i.e., (12)), that describes the motion of the haltere is approximately linear, then the final trajectory of the haltere would simply be the superposition of the response of the two plots shown. Also, each of these plots would scale in proportion to the magnitude of the associated body rate since the Coriolis forces driving the motion are proportional to the respective body rates. Therefore, by measuring the slope and the magnitude of the response near the peak of the haltere trajectory, and having tuned in the appropriate proportionality constants, the body rate components in the plane of the haltere motion could be directly obtained. These observations suggest the following hypotheses.

1) A system with halteres uses the magnitude of the averaged strain at the peak of the haltere stroke and takes advantage of the approximate linearity of the haltere dynamics to estimate Ω_1 (i.e. Ω_1 is proportional to the averaged magnitude of the strain at the middle of the stroke).

2) A system with halteres uses the magnitude of the averaged strain rate at the peak of the haltere stroke and takes advantage of the approximate linearity of the haltere dynamics to estimate Ω_3 (i.e. Ω_3 is proportional to the averaged magnitude of the strain rate at the middle of the stroke).

Pringle[4] demonstrated that the nerve afferents at the end of the stroke are dominated by signals associated with haltere motion reversal. This supports the supposition that the sensory response of the haltere toward the middle of the stroke is of primary use by insects. The proposed method of determining the body rates is more direct than that patented by Wu and Wood.[8] In their patent, the fundamental frequency doubling is taken advantage of through a demodulation scheme to separate the two signals and determine the driving forces. The method proposed here may be directly realizable using the fields of strain sensors (campaniform sensilla) existing at the base of the haltere in insects.

The described mechanism for measuring the body rates requires three characteristics of (12).

1. Linearity
2. No dependence on the out-of-plane body rate Ω_2
3. Two independent forcing functions proportional to the in-plane body rate components Ω_1 and Ω_3

If these characteristics are met, the response to the two in-plane body rate components are uncoupled and the two independent responses are linearly proportional to the magnitudes of the respective body rates. By making various approximations associated with small displacement angles and the magnitudes of the various coupling terms, (12) can be reduced to two possible forms that express the desired characteristics,

$$\ddot{\theta} + 2\zeta\omega_n\dot{\theta} + (\omega_n^2 + \dot{\gamma}^2)\theta = 2\dot{\gamma}\Omega_3\cos(\gamma) + 2\dot{\gamma}\Omega_1\sin(\gamma) \tag{13}$$

$$\ddot{\theta} + 2\zeta\omega_n\dot{\theta} + \omega_n^2\theta = 2\dot{\gamma}\Omega_3\cos(\gamma) + 2\dot{\gamma}\Omega_1\sin(\gamma). \tag{14}$$

The difference between these two equations is simply a centripetal ($\dot{\gamma}^2$) term associated with the out-of-plane motion.

An open question is whether either (13) or (14) are a valid approximation of the full non-linear equation. Comparative simulations were performed between (12), (13) and (14). The closeness of the two darker curves in Figure 8 demonstrate that the first form of the linear approximations in (13) is a fairly accurate representation of the haltere response, unlike the results from (14) which are plotted in the lighter color. Since (13) is a good approximation, the natural decoupling of the trajectories is assumed a generally valid assumption.

V. Error Analysis

An error analysis was performed to demonstrate the limitations the non-linear and out-of-plane cross-coupling terms imposed on the linear approximation of (13). Simulations were executed over a full range of pitch and yaw body rates (i.e., $-20 \leq W_2 \leq 20$ and $-20 \leq W_3 \leq 20$ rad/s). These rates were transformed into the coordinate systems for each of the halteres and then the dynamics for the haltere were simulated using

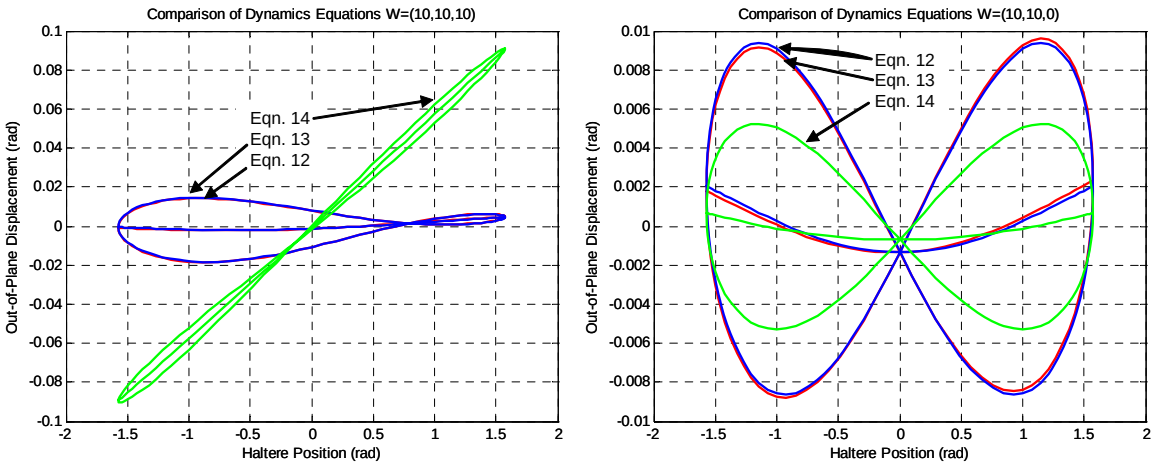

Figure 8. Comparison of the linear simplifications represented by Eq.13 (red) and Eq.14 (green) with the non-linear Eq.12 (blue).

the full non-linear model in (12). Using best estimates of the strain rate and strain magnitude proportionality constants (i.e., constants found to give near zero error for an idealized linear model) the body rates in the haltere frames were estimated. The estimates from the two halteres were then combined using (9), (10), and (11) to reconstruct an estimate for the roll, pitch and yaw rates in the body frame. Each plot represents errors associated with 1681 combinations of yaw and pitch rate for a fixed roll rate. The error is the difference between the exact input body rates and the estimated body rates as demonstrated in Figure 9.

Figure 10 depicts the absolute errors for the pitch, yaw, and roll components of the body rates for the case of critical damping ($\zeta = 1$) and 400 Hz out-of-plane natural frequency. Figure 11 shows the errors for the case where the body roll rate is 5 rad/s.

The change in characteristics shown in Figure 11 can be explained by examining the governing equations of motion in (12). The terms involving Ω_2, which is the out-of-plane rate component and the component most closely aligned with the body roll axis, are summarized below after assuming a small out-of-plane displacement angle, θ.

$$-2\dot{\gamma}\Omega_2\theta + \Omega_2^2\theta + \Omega_2\Omega_3\cos(\gamma) + \Omega_1\Omega_2\sin(\gamma). \tag{15}$$

Since θ is small, the last two terms in (15) will dominate. Note that $\cos(\gamma)$ will always be positive for all stroke angles γ and will be symmetric around $\gamma = 0$. Therefore, the term involving $\cos(\gamma)$ will influence the magnitude of the out-of-plane displacement at $\gamma = 0$ (i.e., the term will influence the yaw error). The term is also proportional to Ω_3, which is closely aligned with the body pitch axis. Therefore, roll coupling will introduce error in the yaw rate estimate that is proportional to the pitch rate. This linear relationship between yaw rate estimation error and pitch rate is exactly what is depicted in the left hand plot in Figure 11. Similar arguments, accounting for the influence of the $\sin(\gamma)$ function on the slope of the haltere out-of-plane motion at $\gamma = 0$ and the proportionality of pitch rate estimation error to the body yaw rate Ω_2, can be made to readily explain the second plot in Fig. 11. The similarity of the third plots in Figures 10 and 11 indicate that the errors from the two halteres cancel, leaving the roll estimate error unaffected by roll rate.

VI. Conclusions

This paper demonstrates the mathematical relationships by which a haltere pair can be used to determine the rotation rate components around the pitch, yaw and roll body axes. The general equation of motion for the haltere that allows out-of-plane response, and therefore accounts for the strains at the base of the haltere, was demonstrated to be approximately linear. By extension of this linearity, the haltere response was shown to be approximately the superposition of the responses to the Coriolis forces caused by the two orthogonal rate components, Ω_1 and Ω_3. Since the Coriolis forces are proportional to Ω_1 and Ω_3, the haltere total response is the superposition of responses that are proportional to Ω_1 and Ω_3. Another implication of the linearity is that Ω_1 is proportional to the magnitude of the haltere displacement at the peak of the

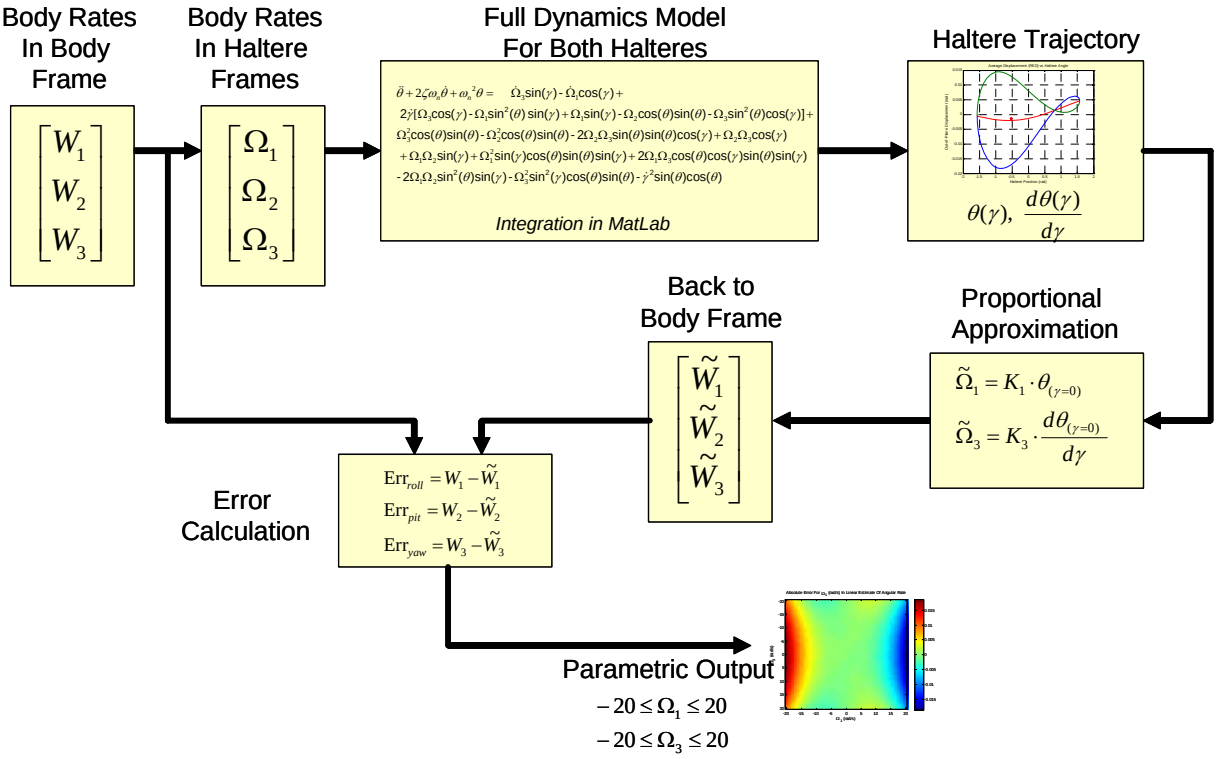

Figure 9. The Error Analysis compared the true rate components along the roll, pitch, and yaw body axis with those reconstructed using the proportional assumptions described in the text. Results are reported as absolute error in radians/sec.

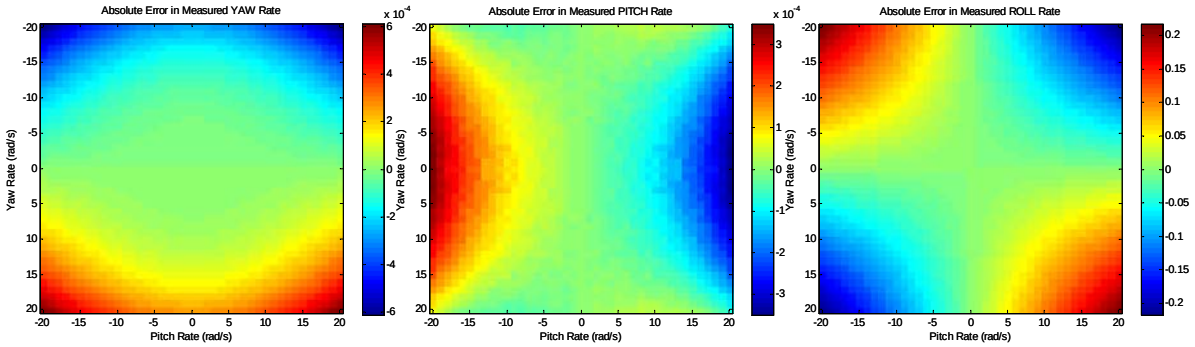

Figure 10. Error in estimates of rate components along the body Yaw, Pitch, and Roll axes for case Roll Rate =0. Conditions vary over a range of -20 to 20 rad/s for the true yaw and pitch rates.

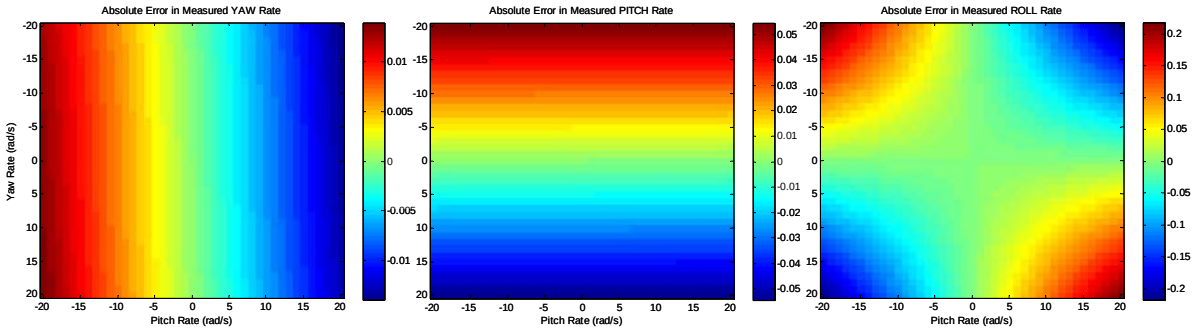

Figure 11. Error in estimates of rate components along the body Yaw, Pitch, and Roll axes for case Roll Rate =5 rad/s. Conditions vary over a range of -20 to 20 rad/s for the true yaw and pitch rates.

haltere stroke and that Ω_3 is proportional to the slope or rate of change of the haltere displacement near the top of the stroke.

An error analysis was performed to demonstrate how accurate the assumed proportionality was when compared to the true values while simulating the full non-linear equation of motion. The idealized haltere model with well tuned proportionality constants had errors for pitch and yaw rate of less than a thousandth of a radian per second over a pitch and yaw rate range of -20 to +20 radians per second. These errors are bounding values since they include no noise or other errors in measurement of the haltere displacement/strain. The results are purely a measurement of the impact of the non-linear coupling in the true equation of motion. The measurement of roll rate had significantly higher errors as shown by Figure 10, which had zero true roll rate. When the roll rate was increased to 5 rad/s the errors in pitch and yaw estimates increased significantly, demonstrating the importance of roll coupling into the dynamics of the haltere. However, it is still possible that the errors are low enough that a stabilization loop based on the derived estimation of pitch, yaw and roll rate would still be useful depending on the specific flight characteristics of the object being controlled and the specific design characteristics of the haltere.

A. Appendix

The expression in (12) can be determined by defining two reference frames in addition to the body fixed frame. These frames are related by the stroke angle γ and the out-of-plane displacement angle θ, as shown in Figure 12. When these angles are zero, the three frames are co-aligned. The associated angular velocities are

$$
\begin{aligned}
{}^{e}\vec{\omega}^{b} &= \Omega_1\hat{b}_1 + \Omega_2\hat{b}_2 + \Omega_3\hat{b}_3 && (16)\\
{}^{b}\vec{\omega}^{h} &= \dot{\gamma}\hat{b}_2 && (17)\\
{}^{h}\vec{\omega}^{f} &= \dot{\theta}\hat{h}_1. && (18)
\end{aligned}
$$

The position and velocities, as observed in the various reference frames, of the mass at the end of the haltere (Point 2) are

$$
\begin{aligned}
\vec{P}_{12} &= r\hat{f}_3 && (19)\\
{}^{h}\vec{v}^{2} &= {}^{h}\vec{\omega}^{f} \times \vec{P}_{12} && (20)\\
{}^{b}\vec{v}^{2} &= {}^{h}\vec{v}_2 + {}^{b}\vec{\omega}^{h} \times \vec{P}_{12} && (21)\\
{}^{e}\vec{v}^{2} &= {}^{b}\vec{v}_2 + {}^{e}\vec{\omega}^{b} \times \vec{P}_{12}. && (22)
\end{aligned}
$$

The expressions leading to the acceleration of the haltere relative to the inertial frame are

$$
\begin{aligned}
{}^{h}\vec{a}^{2} &= {}^{h}\vec{\alpha}^{f} \times \vec{P}_{12} + {}^{h}\vec{\omega}^{f} \times {}^{h}\vec{\omega}^{f} \times \vec{P}_{12} && (23)\\
{}^{b}\vec{a}^{2} &= {}^{h}\vec{a}^{2} + 2({}^{b}\vec{\omega}^{h} \times {}^{h}\vec{v}_2) + {}^{b}\vec{\alpha}^{h} \times \vec{P}_{12} + {}^{b}\vec{\omega}^{h} \times {}^{b}\vec{\omega}^{h} \times \vec{P}_{12} && (24)\\
{}^{e}\vec{a}^{2} &= {}^{b}\vec{a}^{2} + 2({}^{e}\vec{\omega}^{b} \times {}^{b}\vec{v}_2) + {}^{e}\vec{\alpha}^{a} \times \vec{P}_{12} + {}^{e}\vec{\omega}^{b} \times {}^{e}\vec{\omega}^{b} \times \vec{P}_{12}. && (25)
\end{aligned}
$$

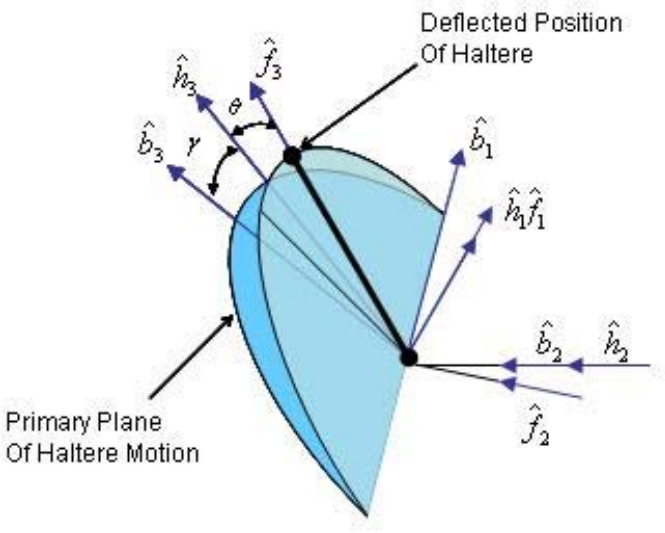

Figure 12. The relative orientation of the reference frames associated with the equation of motion derivation are shown above. The "h" frame is rotated by angle γ with respect the "b" frame. The "f" frame is rotated by angle θ with respect to the "h" frame.

The expression in (25) assumes that the acceleration of the body (Point 1) is small relative to the relevant haltere acceleration terms. This results in the acceleration of point 2 with respect to the earth (inertial) frame in the $\hat{f}_2$ direction as

$$\begin{aligned} \hat{f}_2 \cdot^e \vec{a}^2 \quad = \quad & r[\dot{\Omega}_3 \sin(\gamma) - \dot{\Omega}_1 \cos(\gamma) - \dot{\gamma}^2 \cos(\theta)\sin(\theta) \\ & +2\dot{\gamma}[(\Omega_3 \cos(\gamma) + \Omega_1 \sin(\gamma))\cos^2(\theta) - \Omega_2 \cos(\theta)\sin(\theta)] \\ & +(\Omega_3^2 \cos^2(\gamma) + \Omega_1^2 \sin^2(\gamma) - \Omega_2^2)\cos(\theta)\sin(\theta) \\ & +(\Omega_2\Omega_3 \cos(\gamma) + \Omega_1\Omega_2 \sin(\gamma))\cos(2\theta) \\ & +2\Omega_1\Omega_3 \cos(\theta)\sin(\theta)\cos(\gamma)\sin(\gamma) - \ddot{\theta}]. \end{aligned} \tag{26}$$

The final expression in (12) is obtained by taking the dot product of the inertial force, $-m^e\vec{a}^2$, in the direction of the out-of-plane deflection ($\hat{f}_2$) and then adding the forces associated with stiffness and damping to create a zero sum as

$$\hat{f}_2 \cdot (\vec{F}_{inertial} + \vec{F}_{damping} + \vec{F}_{stiffness}) = 0. \tag{27}$$

Since $r\theta$ increases in the negative $\hat{f}_2$ direction, the stiffness and damping forces were defined as

$$\hat{f}_2 \cdot \vec{F}_{damping} = rm2\zeta\omega_n\dot{\theta} \tag{28}$$

$$\hat{f}_2 \cdot \vec{F}_{damping} = rm\omega_n^2\theta. \tag{29}$$

The resulting expression was divided by the product of the radius of gyration and mass to put it in the final non-dimensional form as

$$\frac{-\hat{f}_2 \cdot^e \vec{a}^2}{r} + 2\zeta\omega_n\dot{\theta} + \omega_n^2\theta = 0. \tag{30}$$

References

[1]Wehner, R., "Polarization vision - a uniform sensory capacity?" *Journal of Experimental Biology*, Vol. 204, 2001, pp. 2589–2596.

[2]Stavenga, D. G. and Arikawa, K., "Evolution of Color and Vision of Butterflies," *Journal of Arthropod Structure and Development*, Vol. 35, 2006, pp. 307–318.

[3]Field, L. H. and Matheson, T., "Chordontal Organs of Insects," *Advances in Insect Physiology*, Vol. 27, Feb. 1998, pp. 1–230.

[4]Pringle, J. W. S., "The Gyroscopic Mechanism of the Halteres of Diptera," *Philosophical Transactions fo the Royal Society B: Biological Sciences*, Vol. 233, Nov. 1948, pp. 347–384.

[5]Gould, A., "Hox/homeotic genes and anterior-posterior patterning," On-line Briefing, agould@nimr.mrc.ac.uk.

[6]Dickinson, M. H., "The Initiation and Control of Rapid Flight Maneuvers in Fruit Flies," *The Journal of Integrative and Comparative Biology*, Vol. 45, April 2005, pp. 274–281.

[7]Sherman, A. and Dickinson, M. H., "A comparison of visual and haltere-mediated equilibrium reflexes in the fruit fly," *The Journal of Experimental Biology*, Vol. 206, Jan. 2003, pp. 295–302.

[8]Wu, W.-C. and Wood, R., "Angular rate sensor using micro electromechanical haltere," United States Patent 7107842, Sept. 2006.

[9]Fraenkel, G. and Pringle, J. W. S., "Halteres of Flies as Gyroscopic Organs of Equilibrium," *Nature*, Vol. 141, 1938, pp. 919–920.

[10]Dickinson, M., "Haltere-mediated equilibrium reflexes of the fruit fly, Drosophila melanogaster," *Philosophical Transactions of the Royal Society B: Biologoical Sciences*, Vol. 354, May 1999, pp. 903–916.

[11]Hengstenberg, R., "Controlling the fly's gyroscopes," *Nature*, Vol. 392, April 1998, pp. 757–758.

[12]Nalbach, G., "The halteres of the blowfly Calliphora I. Kinematics and dynamics," *Journal of Comparative Physiology A*, Vol. 173, Sept. 1993, pp. 293–300.

[13]Faust, R., "Untersuchungen sum Haleterenproblem," *Proc Zool Jahrb Physiol*, Vol. 63, 1952, pp. 325–366.